Climate change intensified heavy monsoon rain in Pakistan, exacerbating urban floods that impacted highly exposed communities

Authors

Mariam Zachariah, *Centre for Environmental Policy, Imperial College, London, UK*
Fahad Saeed*, Climate Analytics, Germany; Weather and Climate Services, Islamabad, Pakistan*
Ben Clarke, *Centre for Environmental Policy, Imperial College, London, UK*
Joyce Kimutai, *Centre for Environmental Policy, Imperial College, London, UK*
Sumayya Ijaz*, Weather and Climate Services, Islamabad, Pakistan.*
Khadija Irfan*, Weather and Climate Services, Islamabad, Pakistan.*
Atta Ullah*, Weather and Climate Services, Islamabad, Pakistan.*
Anwar Sadad, *Weather and Climate Services, Islamabad, Pakistan.*
Israr Ahmad, *Weather and Climate Services, Islamabad, Pakistan.*
Irfan Ur Rashid, *Pakistan Meteorological Department, Pakistan.*
Roop Singh, *Red Cross Red Crescent Climate Centre, The Hague, The Netherlands (based in New Jersey, USA)*
Maja Vahlberg, *Red Cross Red Crescent Climate Centre, The Hague, the Netherlands (based in Ubmeje/Umeå, Sweden)*
Cornelia Scholz*, Red Cross Red Crescent Climate Centre, The Hague, the Netherlands*
Nick Julien Baumgart, *Dept. of Public Health, Copenhagen Centre for Disaster Research, University of Copenhagen*
Emmanuel Raju, *Dept. of Public Health, Copenhagen Centre for Disaster Research, University of Copenhagen*
Friederike Otto, *Centre for Environmental Policy, Imperial College, London, UK*

Review authors

Sarah Kew, *Royal Netherlands Meteorological Institute (KNMI), De Bilt, The Netherlands*
Dora Vrkić, *Grantham Institute - Climate Change and the Environment, Imperial College London, London, UK*

Main findings

- Multiple storms have affected northern Pakistan since the beginning of the monsoon season in June. Flash floods have killed 300 people and injured 715, as of August 3. Nearly half of the deaths are children. In the region studied, 240 people lost their lives.The high death toll highlights the particular vulnerability of children and urgent need to increase resilience to flooding in Pakistan.

- In today's climate, which has warmed by 1.3°C, this event is not particularly rare from a meteorological perspective, with an estimated return period of approximately five years, based on observational datasets.
- Historical trends associated with global warming in observational datasets show the 30-day maximum rainfall over the study region is now approximately 22% more intense than it would have been in a climate that had not warmed by 1.3°C, due to the burning of fossil fuels, and, to a smaller extent, deforestation.
- To quantify the role of human-induced climate change in the observed changes, we analysed trends in climate models. The models show an increase in intensity of extreme rainfall of about 12%, which is smaller than the trend found in observations, in agreement with previous studies in the region. Climate model performance is known to be poor in the region due to the complexity of the drivers of extreme monsoon rainfall, which models struggle to reproduce.
- The majority of models and observations we have analysed show that similar intense rainfall has become heavier as Pakistan has warmed. In particular, two of the climate models included in this analysis, both known for their more realistic representation of aerosols and irrigation that are major factors influencing rainfall processes in this region, were found to show increases of 40-80%. This is in line with the increase found based on observations. The synthesised results indicate that present day climate change has increased the rainfall intensity by around 15% but uncertainties are large, meaning a much larger increase cannot be excluded.
- The findings up till now are corroborated by projections of future 30-day heavy rainfall. Under a 2.6 °C warmer climate compared to preindustrial levels, 30-day heavy rainfall events such as this one are expected to become more frequent and intense.
- While the uncertainties in the results are high, the results are well aligned with published literature on historical trends in monsoon rainfall in Pakistan and projections from the Intergovernmental Panel on Climate Change.
- Pakistan is the fifth most populated country in the world and one of the fastest urbanising countries in South Asia due largely to rural-urban migration within the country. Nearly half of Pakistan's 96.4 million urban residents live in informal settlements. Homes in these areas are often built on riverbanks, drainage basins, and dry riverbeds and are thus at high-risk of flooding. The settlements are typically built from mud and rice husk, making them highly vulnerable. A total of 164 of the flood deaths as of August 3 have been caused by house collapses. Weak enforcement of building codes, deforestation, and building in floodzones amplify the scale of damage, especially in urban centers.
- Adaptation solutions such as nature based solutions (e.g. reforestation, restoring wetlands) that can absorb floodwater, rigorous land use planning and discouraging construction in high-risk areas can reduce the number of people exposed to deadly floods, and enhanced flood early warning and early action systems can help people move out of harm's way in future floods.
- Following the devastating 2022 floods, an estimated USD 16.3 Billion was required for rehabilitation and reconstruction in a resilient way, with donors pledging more than USD 8.5 billion, mostly as loans, and the Pakistan government meeting the remaining requirements. However, this event shows that there is an imperative to not just rebuild but also to adapt to the rising risks. Pakistan is estimated to need USD 152 Billion for adaptation between 2023 and 2030, the majority of which remains unfinanced.

1 Introduction

Torrential monsoon rains around the 16th of July led to devastating floods across Punjab, Pakistan's most populous province, causing widespread destruction and loss of life, primarily from collapsing buildings, and as a result of floodwaters surging through cities and rural areas alike. In Rawalpindi, adjacent to the capital Islamabad, around 230 mm of rainfall fell in less than a day on 17th of July, and overwhelmed drainage systems led to submerged roads, traffic chaos, and floodwater entering homes and businesses (The New York Time, July 18, 2025; Arab News, 17 July 2025). This disaster highlights Pakistan's vulnerability to the human-induced climate crisis, as the country of over 230 million faces extreme weather from both intense heatwaves and heavy monsoon rains (CNN, July 18, 2025). Many deaths were reported in the cities of Lahore and Faisalabad and the towns of Okara, Sahiwal, Pakpattan and several more (Al Jazeera, 17 July 2025).

Monsoon rains are the lifeline of South Asia, essential for irrigation and the replenishment of water resources. However, their adverse impacts have intensified in recent years, exacerbated by rapid urban expansion, inadequate drainage infrastructure, and the increasing frequency of extreme weather events linked to climate change. Pakistan remains especially vulnerable, having experienced the worst flooding in the country's history in 2022 (Otto et al., 2023) with more than 1,700 people killed and an estimated $40 billion in economic damages (UN, 2025). Since 26 June 2025, monsoon-related rainfall has impacted much of Pakistan, triggering floods, landslides, and severe weather incidents that have resulted in significant loss of life and widespread damage.

According to the NDMA Sitreps, as of August 3, the highest number of deaths were reported in Punjab with 162 fatalities, followed by Khyber Pakhtunkhwa (KP) with 70 fatalities. Sindh, Balochistan, Giligit Baltistan (GB), Azad Jammu & Kashmir (AJ&K) and Islamabad Capital Territory (ICT) reported a cumulative death toll of 68 individuals. Additionally, 715 injuries were reported across the provinces, with the highest number of injuries (571 people) occurring in Punjab. The damages to roads stood at 652km, with the highest damages reported in KP where 634km of roads were impacted. GB reported the highest number of damages to bridges rounding at 60 of 105 damaged throughout Pakistan. A total of 1,676 houses were reported to be damaged (including full and partial damages). The highest number was reported in GB with 543 houses damaged followed by 349 in KP, 345 in AJ&K, 214 in Punjab, 87 in Sindh, 82 in Balochistan and 56 in ICT.

According to Pakistan Meteorological Department's (PMD) climate summary report for July 2025, the national area-averaged rainfall estimated at 77.70 mm was above average with a positive anomaly of +23%. However, a diverse situation was observed on a regional scale with Punjab receiving +57% more rainfall, making it 8th wettest July since 1978. Gilgit Baltistan also received 52% more rainfall in July this year. During the month, Pakistan experienced heavy to extremely heavy rainfall in Punjab, Khyber Pakhtunkhwa, Gilgit-Baltistan and Kashmir. It is important to note that on 5th July, Chilas (Gilgit-Baltistan) in northern Pakistan saw a record breaking maximum temperature of 48.5°C.

1.1 Rainfall extremes in Pakistan

The South Asian Monsoon occurs from June to September each year, bringing heavy rainfall to most of the subcontinent. Pakistan is on the far western edge of the South Asian monsoon region, with a mostly arid desert climate in the southern provinces and humid to the north (Ahmed et al., 2019). From June to September, Pakistan often receives heavy rainfall, especially in the northern parts of the country, with over half a million people affected by flooding annually (Baqir et al., 2012). However, it is usually not affected by monsoon low pressure systems, and generally receives far less rainfall than parts of India at the same latitudes. As a result, precipitation rates in Pakistan are extremely variable (Adnan et al., 2021; Ali et al., 2020).

The drivers of extreme rainfall in the region are complex. Past intense monsoons in both India and Pakistan are linked to strong La Niña events but may also occur in neutral or El Niño years (Safdar et al., 2019; Ju & Slingo, 1995). Furthermore, Pakistan is located at a place where two precipitation bearing weather systems terminate - the monsoon rains from east and southeast during summer, and the westerly disturbances from the Mediterranean Sea during winter. It is well established that climate change results in increasing the variability of these systems (Douville et al., 2021). These changes, either spatially or temporally, make the country more prone to such extremes.

In recent years. Pakistan has experienced several severe monsoon seasons resulting in widespread and destructive flooding. In 2010 and 2022, huge swathes of land were flooded across the nation, primarily due to excessive swelling of the Indus River. So far in 2025, the damage was caused by flash flooding from isolated bursts of rainfall rather than widespread riverine flooding as in these other years. However, the origin of these phenomena is similar: consistent, heavy monsoonal rainfall over its western edge, falling as multi-day pulses of extreme rainfall which lead to localised flooding and saturate soil over time (You et al., 2024). Such events are therefore important learning experiences.

In 2022, World Weather Attribution undertook a probabilistic rapid analysis of the heavy precipitation that drove the flooding (Otto et al., 2022), which was later peer-reviewed (Otto et al., 2023). At the time, this included a review of the scientific understanding of changes in extreme rainfall in the South Asian monsoon over Pakistan. Drawing from the IPCC and wider scientific literature, including several studies on the 2010 flooding, this initial review found the following: (i) there are robust observed increasing trends in extreme precipitation over the wider South Asia (IPCC) region and westward movement of the monsoon over Pakistan, but (ii) there was overall low confidence in the attribution of this to human influence on the climate, as a result of other factors such as irrigation practices, local aerosols, and large-scale atmospheric circulation also driving the net trends. Furthermore, (iii) projections indicated that it was linked to a stronger and more variable South Asian monsoon, but this was not isolated to the Pakistan region only, suggesting the need for subregional analysis (Otto et al., 2023).

The WWA study then analysed changes in shorter multi-day (5-day) and longer seasonal (60-day) extreme precipitation over the southern provinces of Balochistan and Sindh, and the wider Indus basin, respectively. In accordance with the wider literature, it found strong increasing trends in observed extreme precipitation, which suggested an increase of 75% and 50% in the intensity of such 5-day and 60-day events, respectively. A full attribution was not possible, due to the failure of many state-of-the-art climate models to capture key processes driving precipitation in the region. Combining the available evidence, the report concluded that the 5-day event over the southern parts of Pakistan was likely amplified by climate change with a possible intensity change of up to 50%, while the influence on the 60-day event over the Indus Basin was uncertain.

Beyond the hazard analysis, the report found that the impacts were also driven by the proximity of human settlements (homes, buildings, bridges) and agricultural land to flood plains, inadequate infrastructure, limited ex-ante risk reduction capacity, an outdated river management system, underlying vulnerabilities driven by high poverty rates and socioeconomic factors (e.g. gender, age, income, and education), and ongoing political and economic instability. Finally, it concluded that increasing observed trends underlined the importance of reducing vulnerability and exposure to extreme events in Pakistan (Otto et al., 2023).

Other recent studies have also explored the drivers of this event. One study found that (cross-equatorial) moisture transport from the Arabian sea into Pakistan during the monsoon has exhibited an increasing trend since the 1960s. In 2022, this anthropogenically-driven trend in moisture transport combined with La Niña and negative IOD conditions to create an atmospheric channel of moisture into Pakistan that sustained the westward-travelling low-pressure systems (You et al., 2024). This moisture transport may have been amplified by the late spring thermal low, which in turn was amplified by anthropogenic forcing (Otto et al., 2023). Using an operational forecast-based approach, another study found that anthropogenic forcing (increases in atmospheric CO_2 and ocean temperature) was responsible for about 10% of the rainfall over Pakistan during June-August 2022 (Weisheimer et al., 2025). This was consistent with enhanced southwesterly winds leading to increased moisture transport from the Arabian sea. However, a comparable experiment with future CO_2 levels and ocean temperatures found that the rainfall signal reduced compared to present day levels by approximately 5%. It should also be noted that the variability of the results in the future experiment increased, giving more intense extremes from the highest ensemble members, and weaker extremes in the lowest members (Weisheimer et al., 2025).

To summarise, there is now a clear and present increase in extreme monsoon precipitation in the region, and recent studies have begun to elucidate a link to present day warming of the atmosphere primarily due to human activities. However, the drivers of this hazard both now and in the future and at different scales remain complex and enigmatic, and severe impacts continue to occur in the region. Both of these factors suggest the need for further study of all aspects of risk as a scientific and societal imperative. In this study, we aim to add to this evolving understanding by studying the recent flooding disasters in northern and eastern Pakistan.

1.2 Dynamic assessment of the extreme rainfall spells in 2025

The South Asian Summer Monsoon (SASM) is a highly dynamic and multifaceted atmospheric system governed by a complex interplay of thermodynamic, oceanic, and atmospheric processes operating across various spatial and temporal scales, making it "notoriously difficult to predict" (Jayaraman, 2005; Subramanian, 2021). Based on earlier scientific findings, some of the important dynamical processes impacting SASM include the El Niño–Southern Oscillation (ENSO), Indian Ocean Dipole (IOD), sea surface temperatures (SSTs) in the Arabian Sea and Bay of Bengal, the subtropical jet stream, and the thermal contrast between land and ocean among others (NDMA, 2025).

The devastating floods of 2010 and 2022 in the country's history were found to be influenced by major remote forcings, namely ENSO and the IOD. In both of these years, La Niña conditions prevailed, and the IOD was in its negative phase (Otto et al., 2023), leading to enhanced monsoonal moisture transport and amplified rainfall. However, both ENSO and IOD conditions were neutral in 2025, implying limited influence from these large scale ocean-atmosphere phenomena in driving rainfall anomalies this year.

Nevertheless, Pakistan experienced an intense heatwave during the pre-monsoon period from April to early June 2025, with temperatures rising above 50°C in parts of the country (PMD, 2025). This resulted in high surface heating, contributing to the development of a pronounced heat low over Iran, Afghanistan, and part of Pakistan (Figure 1.1 (a,b)). Unlike the 2022 floods, where pre-monsoon heat anomalies were centered over the Indus basin, this year's heat maximum was located further west (over Iran, Afghanistan, and Pakistan) resulting in the development of a heat low. Saeed et al. (2010) underscored the role of this heat low, which acts as a bridge connecting the mid-latitude wave train to the SASM rainfall through differential heating between land and ocean, and found a significant correlation between the heat low and upper-level mid-latitude circulation.

Figure 1.1 (c, d) further supports this linkage by showing elevated geopotential height anomalies at 200 hPa over Central Asia, consistent with the presence of an upper-level high during the positive phase of the circumglobal wave train in 2025. The concurrent presence of a surface heat low and an upper-level high creates a favorable setting for subsidence leading to thermal amplification, which may have preconditioned the atmosphere for intense and spatially concentrated rainfall later in the season.

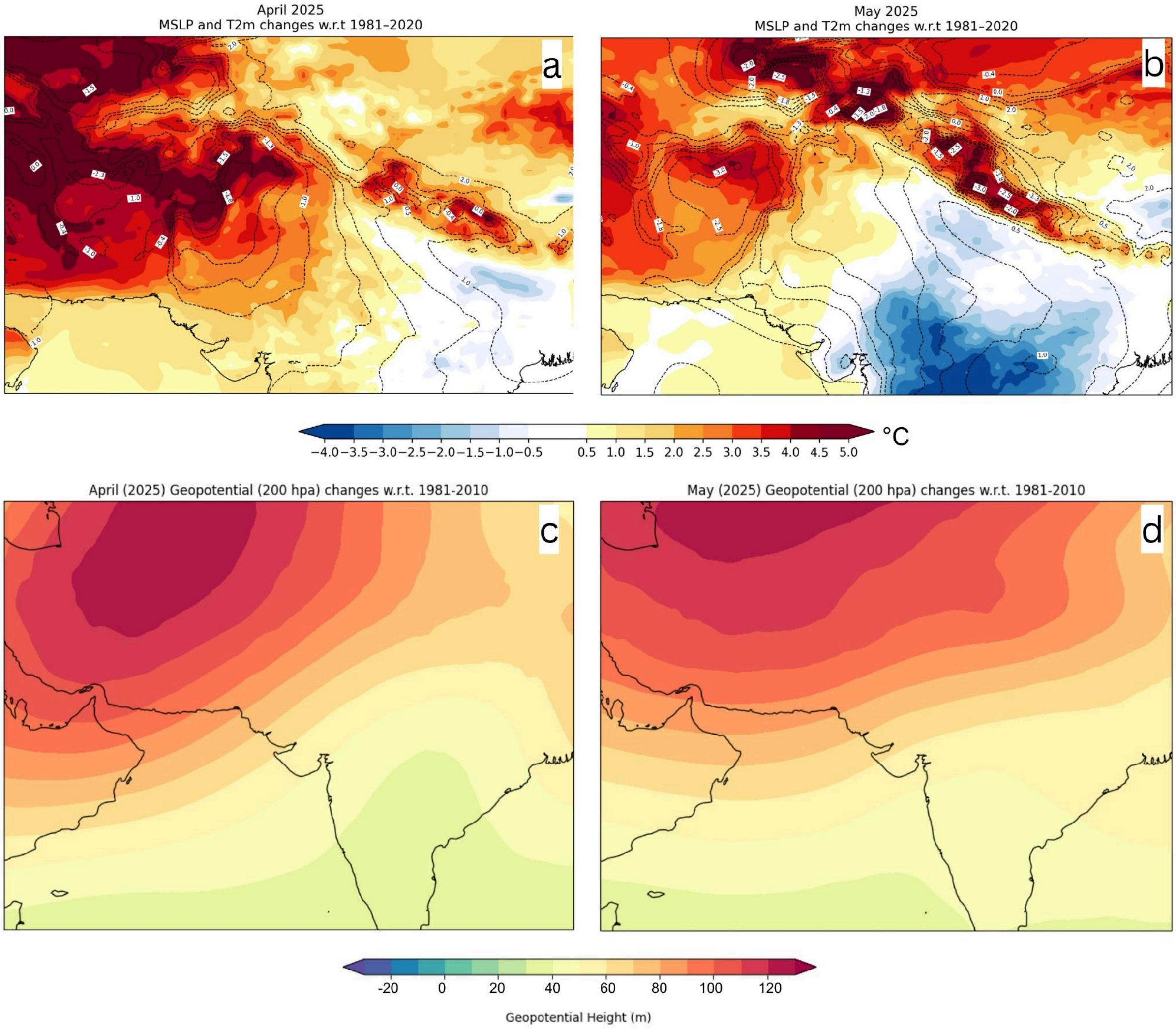

Figure 1.1:* *(a,b) *2m Temperature (shaded) and mean sea level pressure (isobars) anomalies from ERA5* ***(c,d)*** *200 hPa geopotential heights from ERA5*

This upper level anomalous high associated with mid-latitude circulation is also known to impact the SASM systems over northern Pakistan region at intraseasonal time scale. Saeed et al. (2014) developed a similar geopotential height index at 200 hPa over central Asia, which has a significant correlation with the rainfall over the Upper Indus Basin (UIB), as a precursor of the UIB rainfall. Figure 1.2(b) displays the lead-lag correlation plot between the rainfall over the UIB and the geopotential height index from Saeed et al. (2014). Between 26th June and 31st July 2025, four monsoon systems reached our studied region as depicted in Figure 1.2(a) by red filled circles at the days of maximum rainfall during each spell. The geopotential height line shows a peak 2-5 days before the maximum rainfall in three out of four spells, in line with the findings of Saeed et al. (2014). Moreover, Figure 1.2(c) also shows a lead-lag correlation plot between our studied region rainfall and geopotential height index at 200 hPa defined by Saeed et al. (2014) for June-July 2025, with similar patterns as that of Figure 1.2(b).

In summary, the pre-monsoon heat low at the seasonal scale, combined with increased mid-latitude circulation activity over Central Asia, played a significant role in exacerbating this year's rainfall. It is also important to note that, unlike the 2022 event, which brought an unprecedented 700% increase in precipitation over Sindh, this year's rainfall, while intense, was not record-breaking. Furthermore, the rainfall remained largely confined to the core monsoon belt and was influenced by well-known precursory conditions typically associated with such events.

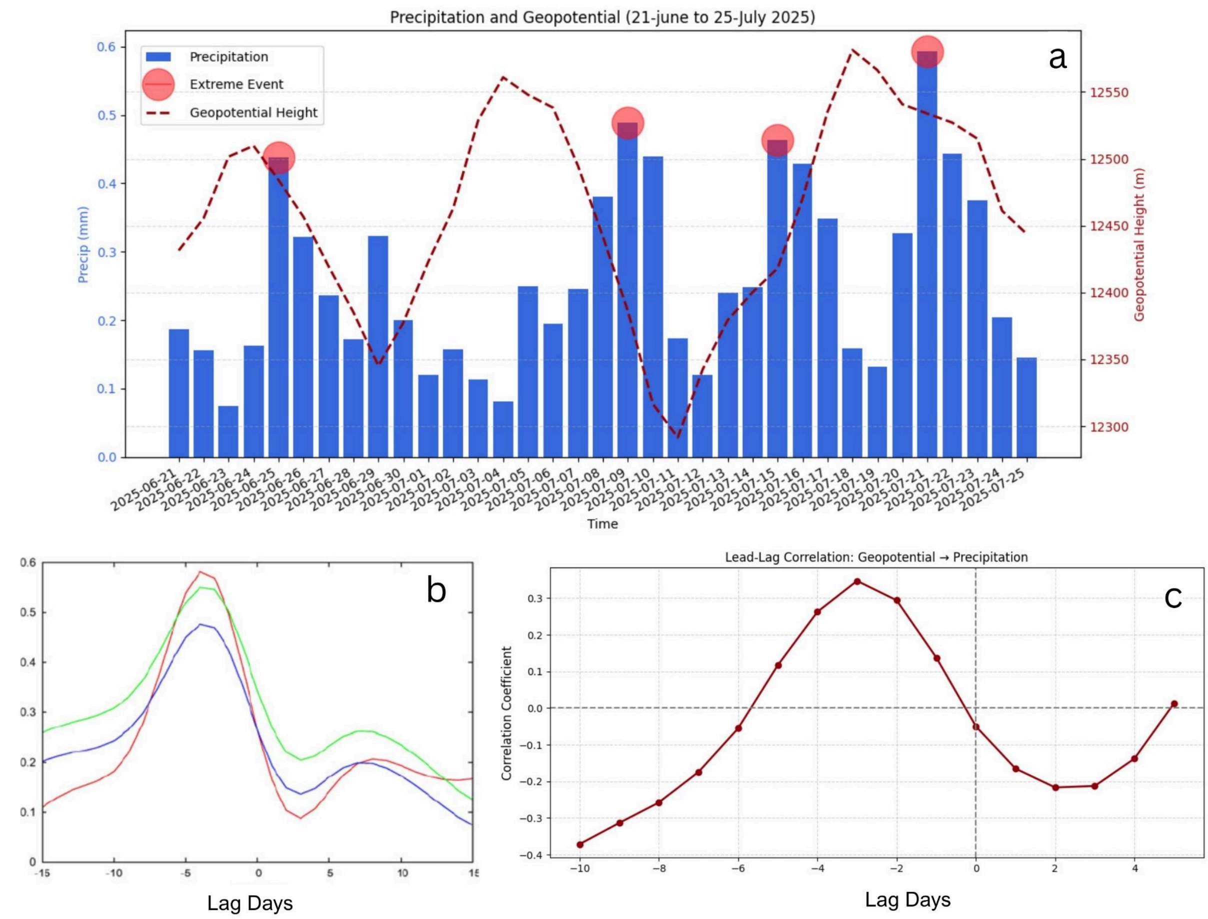

***Figure 1.2: (a)** ERA-5 daily precipitation (blue bars) and geopotential height (red dashed curve) at 200hPa over the domains (PUIB: 70°-80°E, 30°-36°N) and (GH: 65°E-80°E, 35°-45°N) respectively; **(b)** Lead-lag correlation coefficients between GH and PUIB using ERA40 data (red curve), between GH from ERA40 and OLR from NOASS (green curve) and between GH from NCEP and OLR from NOAA (blue curve) for the domains mentioned in panel (a) taken from Saeed et al. (2014); **(c)** Same as in (b) but for GH and PUIB from ERA5 for June and July 2025.*

1.2 Event Definition

To capture the range of impacts from the incessant heavy rainfall that have been battering the northern part of Pakistan (27.52 - 37.37N, 69.13 - 75.51E; bounding box in Fig. 1.3) since the start of the monsoons this year, we choose a considerably long accumulation period of 30 days and focus on the seasonal (JJAS) maximum 30-day rainfall for the temporal extent. For the spatial domain, we focus on a climatologically homogeneous region covering the major impact sites in the provinces of Punjab, Khyber Pakhtunkhwa, Gilgit Baltistan and Azad Kashmir including the cities Islamabad, Rawalpindi, Faisalabad, Sargodha, Sialkot, Swat, Peshawar and Lahore.

Figure 1.3 (a) shows the 30 day rainfall total during the period 24 June - 23 July 2025 when the region received most of the heavy rainfall this year. Most of the heavy rainfall was recorded in the eastern parts of the study area over the Punjab province. Figure 1.3 (b) illustrates the distribution of population across the study area in northern Pakistan. The map clearly shows that the eastern region contains several major urban centers with very high population density. In contrast, the northern mountainous areas are sparsely populated. Notably, valleys within the mountainous regions show higher population concentrations, though this density diminishes further north. The total population within the study area—over 130 million people—was calculated using WorldPop 2020 population estimates, based on population counts within 1 km² grid cells. When assessing the rainfall during this period alongside the population density map, it becomes evident that the most densely populated regions were also the most affected by intense monsoon rainfall. An estimated 106 million people were exposed to rainfall in areas where totals exceeded 200 mm during the 30 day period, based on the overlap between rainfall and population data.

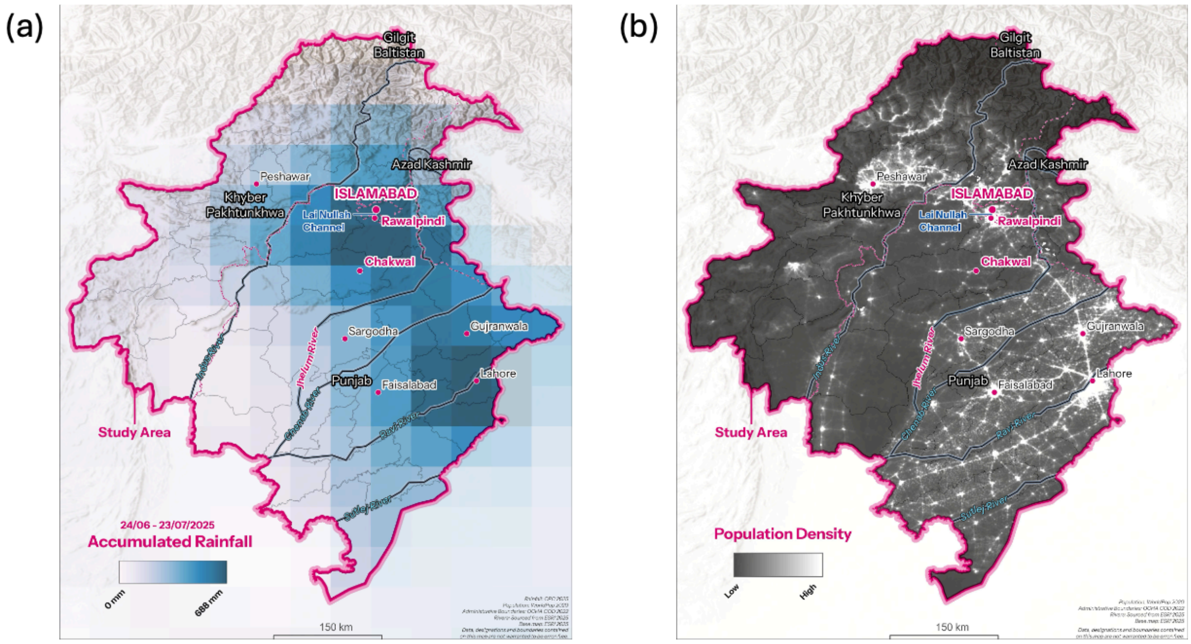

***Figure 1.3[1]: (a)** Accumulated rainfall (in millimeters) recorded between 24 June and 23 July 2025. Rainfall rates are visualized using a gradient of blue shades, with dark blue indicating the highest rainfall (up to 688 mm) and light grey representing the lowest recorded levels. **(b)** Distribution of population across the study area in northern Pakistan. The gradient from white to black represents population density, with white indicating areas of high density, black denoting areas of low density, and varying shades of grey in between.*

In this report, we study the influence of anthropogenic climate change by comparing the likelihood and intensity of similar rainfall extremes at present with those in a 1.3°C cooler climate. We also extend this analysis into the future by assessing the influence of a further 1.3°C of global warming

[1] Depictions of boundaries in this figure and all subsequent figures are for illustrative purposes only and do not imply any official position.

from present. This is in line with the latest Emissions Gap Report from the United Nations Environment Programme, which shows that the world is on track for at least 2.6°C temperature rise given currently implemented policies (UNEP, 2024).

2 Data and methods

2.1 Observational data

We first use observational and reanalysis data to estimate the return period of a similar event in the present day and to assess the historical trends with increasing GMST. The precipitation datasets used are as follows:

- **ERA5** - The European Centre for Medium-Range Weather Forecasts's 5th generation reanalysis product, ERA5, is a gridded dataset that combines historical observations into global estimates using advanced modelling and data assimilation systems (Hersbach et al., 2020). This product has a spatial resolution of 0.5°×0.5°, from the years 1950 to present. The re-analysis is available until the end of the preceding month (June 2025). We extend the re-analysis data with the ECMWF analysis (1-20 July) and the ECMWF forecast (21-25 July) to cover the period of the event.
- **CPC** - This is the gridded product from NOAA PSL, Boulder, Colorado, USA known as the CPC Global Unified Daily Gridded data, available at 0.5° x 0.5° resolution, for the period 1979-present. Data are available from NOAA.
- **MSWEP** - The Multi-Source Weighted-Ensemble Precipitation v2.8 dataset (updated from Beck et al., 2019) is fully global, available at 3-hourly intervals and at 0.1° spatial resolution, available from 1979 to ~3 hours from real-time. This product combines gauge-, satellite-, and reanalysis-based data, including ERA5.
- **CHIRPS** - The rainfall product developed by the UC Santa Barbara Climate Hazards Group called "Climate Hazards Group InfraRed Precipitation with Station data" (CHIRPS; Funk et al. 2015). Daily data are available at 0.05° resolution, from 1981-30 June 2025. The product incorporates satellite imagery with in-situ station data.
- **GPM-IMERG** - This product uses the Integrated Multi-satellitE Retrievals for GPM (IMERG) algorithm for combining information from the GPM satellite constellation to estimate precipitation over the majority of the Earth's surface (Rozante et al. 2010). It is available at a spatial resolution of 0.2° globally from 1st Jan 1998 - 30th April 2025.
- **Pakistan Meteorological Department (PMD) Station data -** Data from 9 PMD stations (Faisalabad, Islamabad, Jhelum, Kakul,Lahore, Murree, Peshawar, Sargodha and Silakot) have also been included in our analysis which ranges from 1960s up to July 2025.

Figure 2.1 shows the 30-day rainfall event from 24 June to 23 July 2025, as captured by each of the selected gridded datasets, overlaid with rainfall values from nine PMD stations located in the study region, where the heaviest rainfall occurred. The station data closely match the spatial patterns seen in the gridded datasets, with slightly lower rainfall recorded at the western stations compared to those in the east. Furthermore, the rainfall patterns in all four datasets (except CHIRPS, which did not have data for this event at the time of writing) were consistent with the interpolated rainfall patterns based on station records for the same period. This consistency provides confidence in the ability of the gridded datasets to accurately capture the event, thus supporting their use in the next step of the analysis.

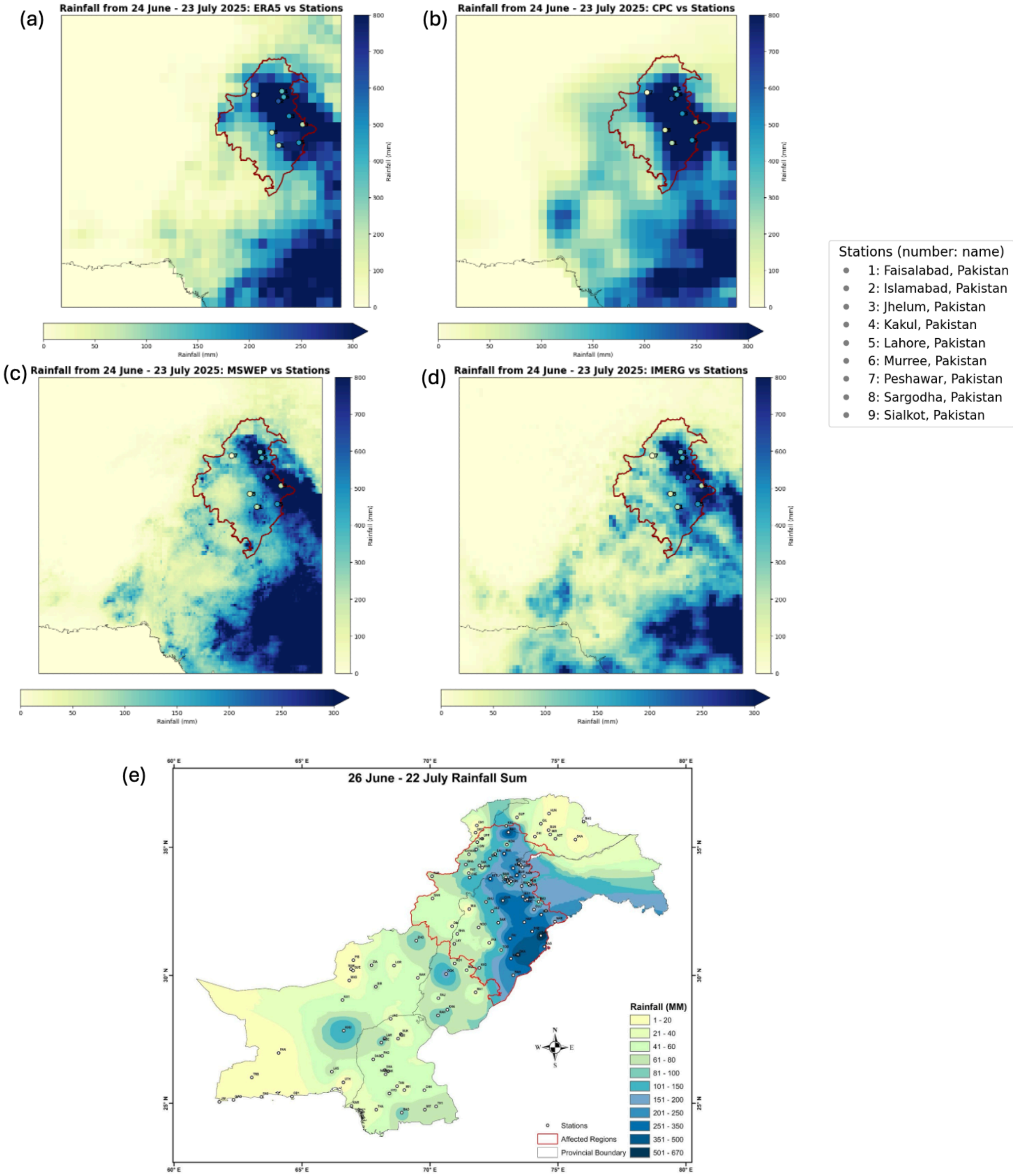

__Figure 2.1__: Rainfall during 24 June- 23 July 2025 in the four gridded datasets which has the event __(a)__ ERA5, __(b)__ CPC, __(c)__ MSWEP and __(d)__ IMERG with the accumulated rainfall during the same period from the nine stations overlaid. __(e)__ Rainfall during 26 June-22 July 2025, plotted from estimates collated from the [NDMA Sitereps](#) since 26 June 2025 on this event.

In addition, as a measure of anthropogenic climate change we use the (low-pass filtered) global mean surface temperature (GMST), where GMST is taken from the National Aeronautics and Space

Administration (NASA) Goddard Institute for Space Science (GISS) surface temperature analysis (GISTEMP, Hansen et al., 2010 and Lenssen et al. 2019).

Finally, as a measure of the El Niño - Southern Oscillation cycle (ENSO) we use the detrended Niño3.4 index. This is computed from NOAA's ERSST v.5 sea surface temperatures, by subtracting the mean tropical SST (20S-20N) from the mean SST over the Nino3.4 region (5S-5N, 170W-120W). This index is therefore adjusted to remove the linear trend associated with climate change as proposed in van Oldenborgh et al., 2021, but without rescaling each calendar month.

2.2 Model and experiment descriptions

We use 3 multi-model ensembles from climate modelling experiments using very different framings (Philip et al., 2020): Sea Surface temperature (SST) driven global circulation high resolution models, coupled global circulation models and regional climate models. These are as follows:

1. Coordinated Regional Climate Downscaling Experiment CORDEX-CORE over the West-Asia domain with 0.22 km resolution (WAS-22) (Teichman et al., 2021). The ensemble consists of 6 regional climate models, each downscaling 4 GCMs. These simulations are composed of historical simulations up to 2005, and extended to the year 2100 using the RCP8.5 scenario.
2. CMIP6. This consists of simulations from 21 participating models with varying resolutions. For more details on CMIP6, please see Eyring et al., (2016). For all simulations, the period 1850 to 2015 is based on historical simulations, while the SSP5-8.5 scenario is used for the remainder of the 21st century.
3. HighResMIP SST-forced model ensemble (Haarsma et al. 2016), the simulations for which span from 1950 to 2050. The SST and sea ice forcings for the period 1950-2014 are obtained from the 0.25° x 0.25° Hadley Centre Global Sea Ice and Sea Surface Temperature dataset that have undergone area-weighted regridding to match the climate model resolution. For the 'future' time period (2015-2050), SST/sea-ice data are derived from RCP8.5 (CMIP5) data, and combined with greenhouse gas forcings from SSP5-8.5 (CMIP6) simulations (see Section 3.3 of Haarsma et al. 2016 for further details).

2.3 Statistical methods

Methods for observational and model analysis and for model evaluation and synthesis are used according to the World Weather Attribution Protocol, described in Philip et al., (2020), with supporting details found in van Oldenborgh et al., (2021), Ciavarella et al., (2021), Otto et al., (2024) and here. The key steps, presented in sections 3-6, are: (3) trend estimation from observations; (4) model validation; (5) multi-method multi-model attribution; and (6) synthesis of the attribution statement.

In this report we analyse time series of the June-September maximum 30-day precipitation over the study region. A nonstationary GEV distribution is used to model this index, and the distribution is assumed to scale exponentially with the covariate GMST, with the dispersion (the ratio between the standard deviation and the mean) remaining constant over time. In particular, the variable of interest, X , is assumed to follow a GEV distribution in which the location and scale parameters vary with GMST, following:

$$X \sim GEV(\mu, \sigma, \xi \mid \mu_0, \sigma_0, \alpha, T),$$

where X denotes the variable of interest, rainy-season precipitation; T is the smoothed GMST; μ_0, σ_0 and ξ are the location, scale and shape parameters of the nonstationary distribution; and α is the trend due to GMST. As a result, the location and scale of the distribution have a different value in each year, determined by both the GMST and Niño3.4 states. Maximum likelihood estimation is used to estimate the model parameters, with

$$\mu = \mu_0 exp\left(\frac{\alpha T}{\mu_o}\right) \quad \text{and} \quad \sigma = \sigma_0 exp\left(\frac{\alpha T}{\mu_o}\right).$$

This formulation reflects the Clausius Clapeyron relation, which implies that precipitation scales exponentially with temperature (Trenberth et.al., 2003, O'Gorman and Schneider 2009). The parameters of the statistical model are estimated using maximum likelihood.

For each time series we calculate the return period and intensity of the event under study for the 2025 GMST and for 1.3°C cooler GMST: this allows us to compare the climate of now and of the preindustrial past (1850-1900, based on the Global Warming Index), by calculating the probability ratio (PR; the factor-change in the event's probability) and change in intensity of the event.

2.3.1 The potential role of ENSO

The El Nino-Southern Oscillation (ENSO) is known to play a modulating role in the relative strength of the South Asian Monsoon in any given year. As a result, it may influence extremes at subregional scales, such as the event studied here. In order to investigate if current ENSO conditions influenced the event, or if taking ENSO conditions into account improved our statistical representation of extremes in the region, the relative Niño3.4 index described in section 2.1 was used as an additional covariate in the model above. The subsequent modified distribution then follows:

$$X \sim GEV(\mu, \sigma, \xi \mid \mu_0, \sigma_0, \alpha, \beta, T, I),$$

where I is the detrended Niño3.4 index and β is the trend due to ENSO, and where

$$\mu = \mu_0 exp\left(\frac{\alpha T + \beta I}{\mu_o}\right) \quad \text{and} \quad \sigma = \sigma_0 exp\left(\frac{\alpha T + \beta I}{\mu_o}\right).$$

The two models were then tested for their relative goodness of fit to the observed time series, using the Akaike information criterion. This metric assesses goodness of fit while also penalising model complexity to avoid overfitting. This indicated that the GMST-only model better represented the extremes in question, suggesting that ENSO plays a limited role for extremes at this particular temporal and spatial scale.

3 Observational analysis: return period and trend

3.1 Analysis of point station data and gridded data

Linear trends in 30-day rainfall spells at individual PMD stations indicate a decreasing tendency in the northern part of the study region in recent years, while stations in the southern part show increasing trends (Fig. 3.1). Among the five gridded datasets analyzed, IMERG and CHIRPS most closely mirror the observed station trends, especially in capturing the drying vs. wetting tendency in the north vs. south of the study region. In contrast, ERA5 and MSWEP exhibit a drying trend, which may partly stem from the limitations in the numerical representation to accurately simulate the complex rainfall patterns in this region, particularly due to its proximity to mountainous terrain. However, MSWEP has a relative advantage over ERA5 in that it is a blended product, incorporating station-based and satellite-based data along with the reanalysis data (ERA5), allowing it to produce near-real-time, high-resolution rainfall records. While CPC includes data from a comparatively large number of stations, its coarser resolution limits its ability to resolve finer-scale variability arising from topographic heterogeneity and local- to mesoscale atmospheric processes. Given these considerations, we choose to include CPC, MSWEP, CHIRPS, and IMERG as independent observational datasets to capture the full range of uncertainty expected in observational rainfall estimates across the study region.

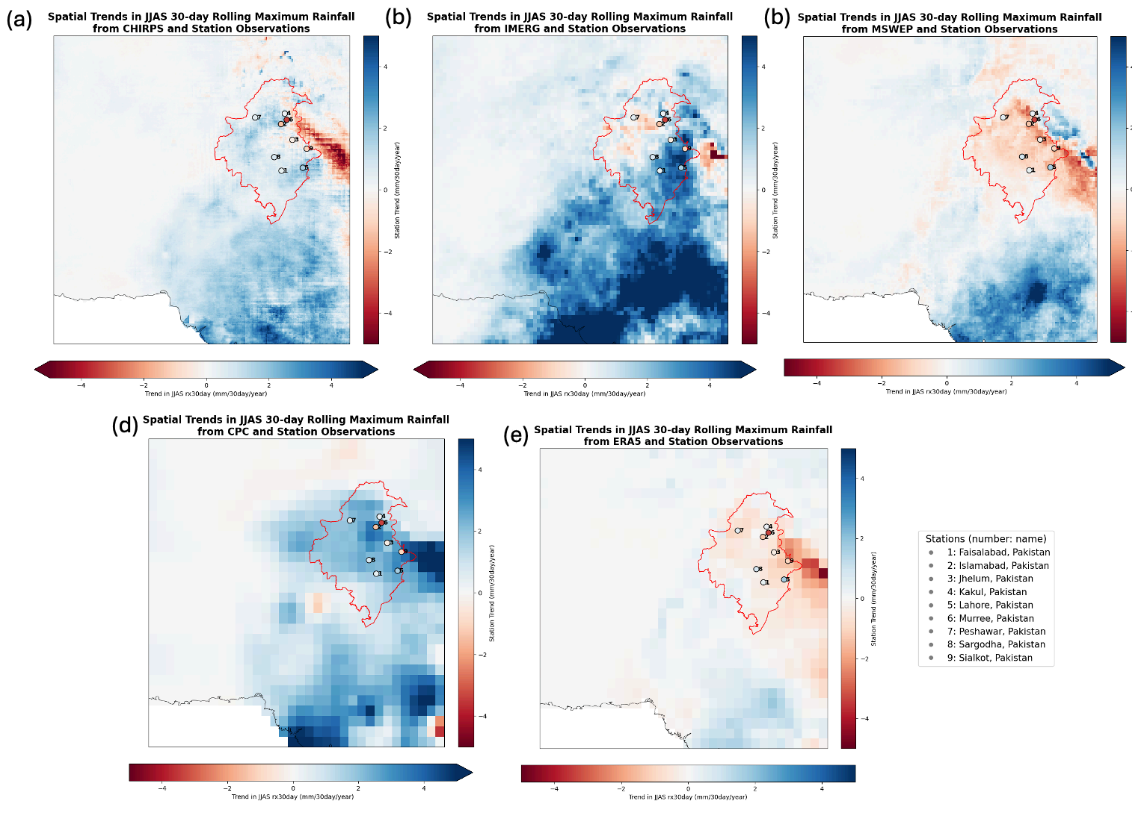

Figure 3.1: *Linear trends in gridded datasets **(a)** CHIRPS, **(b)** IMERG, **(c)** MSWEP, **(d)** CPC and **(e)** ERA5, all compared with in-situ (station) observations*

Table 3.1 summarised the return periods, magnitude of the 30-day rainfall during 24 June-23 July 2025 at 8 stations in the study domain. The station at Murree was dropped from this point on, as this location has been a recipient of land cover change in recent years due to its emergence as a tourist destination. Further, the station in Kakul which also is a station close to Murree is deemed to be a good representative of the mountainous climate. At 4 stations—namely, Faisalabad, Lahore, Peshawar and Sargodha—there are discernible increasing trends suggesting that 30-day rainfall events in the JJAS season such as this one are becoming more intense due to climate change. Kakul station also shows a strong increasing trend, but becomes evident only for heavier events that are more extreme (see Appendix Fig. A1).

Table 3.1: *Change in probability ratio and magnitude for JJAS Rx30day in 8 stations in North Pakistan region due to GMST.*

Station	**Event : JJAS Rx30day**		**GMST (Covariate)**	
	Magnitude (mm/30day)	**Return period (95% C.I.)**	**Probability Ratio**	**Change in magnitude (%)**
Faisalabad	221.13	4 (2...7)	2.145 (0.74...389.305)	21.836 (-8.368...85.62)
Islamabad	621.22	6 (4...56)	0.599 (0.028...2.103)	-10.675 (-43.132...18.024)
Jhelum	497.43	8 (5...31)	1.195 (0.267...3.502)	3.831 (-21.844...25.467)
Kakul	355	2 (1...3)	4.003 (-17.665...20.573)	1.145 (0.51...2.406)
Lahore	488.31	10 (4...35)	2.559 (0.802...Inf)	15.352 (-1.89...86.537)
Peshawar	22.43	1 (1...1)	1.006 (0.978...1.019)	29.507 (-56.426...81.232)
Sargodha	131.44	1 (1...2)	1.124 (0.819...2.019)	14.292 (-20.334...81.979)
Sialkot	212.57	1 (1...1)	0.962 (0.814...1.068)	-11.461 (-40.395...21.339)

In gridded observational and reanalysis datasets, all datasets show that the 2025 event had a best-estimated return period of approximately 2-5 years (see Table 3.2 and Fig. 3.1). There is low agreement in the change due to global warming of 1.3°C at present compared to the preindustrial climate. ERA5 and MSWEP suggest an approximate halving of the likelihood of such events, with reductions in intensity by 13-20%. On the contrary, IMERG suggests an approximate doubling and increase in intensity by 24%, while CPC and CHIRPS show statistically significant strong increases in likelihood by a factor of 220 (2.6 - 10^8) and 30 (2.2 - 10^5), respectively, and equivalent increases in intensity by 93% (14 - 190%) and 39% (0.35 - 110%), respectively. On account of the trend in stations reflecting some of the gridded datasets more than the others, we include an estimate based on averaging the 8 stations as an additional independent candidate for the observed trends alongside CHIRPS, IMERG, CPC and MSWEP (see Fig. 3.1). Averaging the rainfall records over the 8 PMD stations, the 2025 event is a 1-in-4 year event in the records; the trends suggest an overall slight increase, albeit much smaller than what is shown in the individual stations. Overall, the trends in the observation-based products (CPC in this case) and the satellite products—CHIRPS and IMERG—are consistent with the station-averaged trends, whereas this is not the case for ERA5 (which is a reanalysis product) and MSWEP; this is not surprising but simply underscores that the complex terrain and the influence of other large-scale circulations in driving rainfall processes in the region is better captured by observations (satellite and stations), and may be inducing limitations in numerical weather modelling algorithms that go into the creation of the reanalysis data.

Based on the return period estimates from the observations, we infer that the event is approximately a 1 in 5 year event and use this return period for subsequent model analysis.

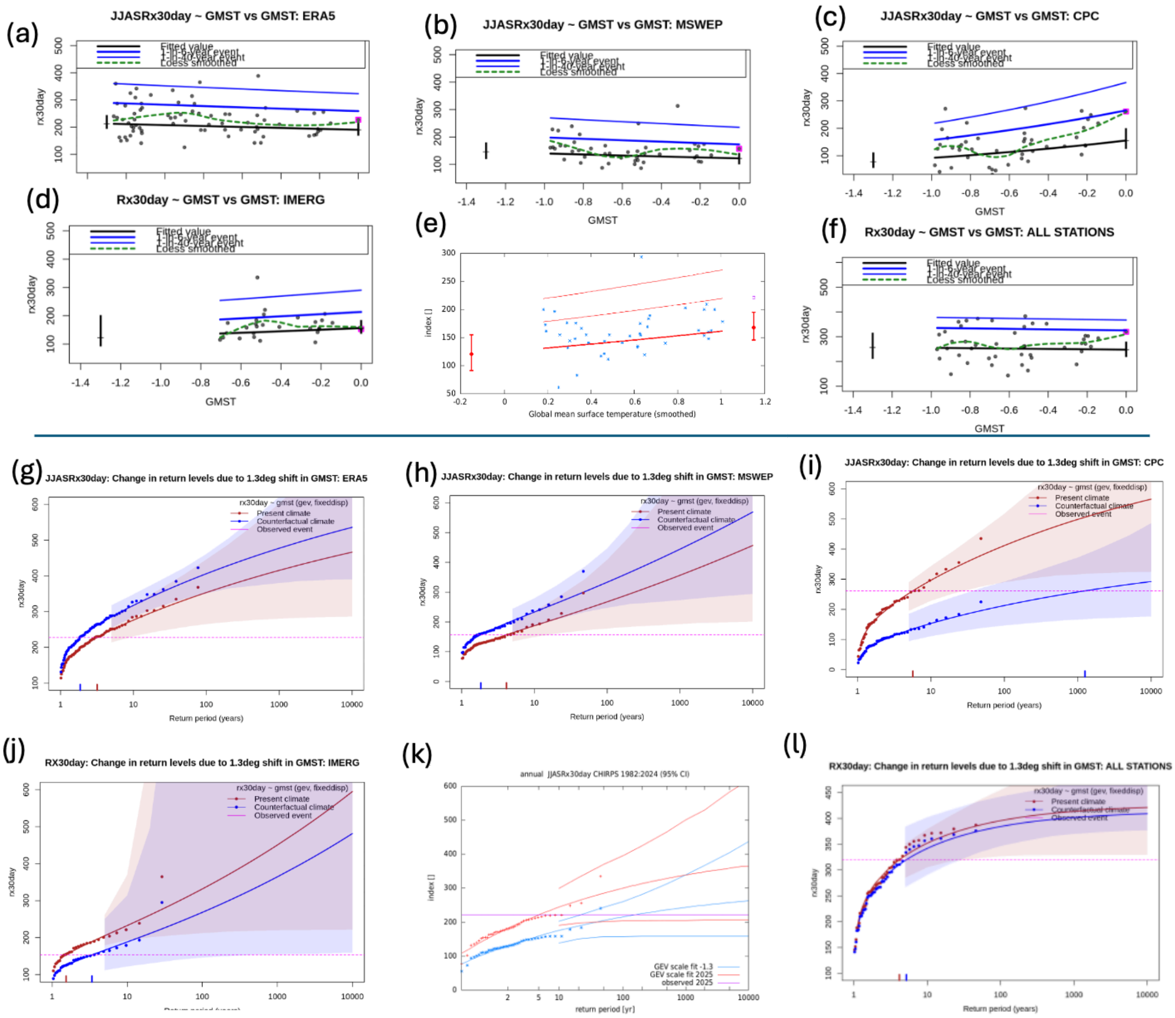

Figure 3.1: *GEV fit with fixed dispersion parameter scaling proportional to GMST of the index series.* ***(a-f)*** *Observed JJAS Rx30day [mm/30day] as a function of the smoothed GMST. The thick black line denotes the time-varying location parameter. The vertical black lines show the 95% confidence interval for the location parameter, for the current, 2025 climate and the fictional, 1.3ºC cooler climate. The 2025 observation is highlighted with the magenta box.* ***(g-l)*** *Return time plots for the climate of 2025 (red) and a climate with GMST 1.3ºC cooler (blue). The past observations are shown twice: once shifted up to the current climate and once shifted down to the climate of the pre-industrial era. The markers show the data and the lines show the fits and uncertainty from the bootstrap. The magenta line shows the magnitude of the 2025 event analysed here. These are shown for ERA5, MSWEP, CPC, IMERG, CHIRPS and the station-average.*

Table 3.2: *Change in probability ratio and magnitude for JJAS Rx30day in North Pakistan region due to GMST. Statistically significant trends are highlighted in colored* ***bold*** *font.*

Dataset	**Event : JJAS Rx30day**		**GMST (Covariate)**	
	Magnitude (mm/30day)	**Return period (95% C.I.)**	**Probability Ratio**	**Change in magnitude (%)**
CPC	261.485	5.0 (3.0 ... 26)	**2.2e+2 (2.6 ... 1.4e+8)**	**93 (14 ... 1.9e+2)**
IMERG	153.255	2.0 (1.0 ... 3.0)	2.2 (0.71 ... 3.9e+2)	24 (-17 ... 98)
Stations	311.899	4.0 (3 … 30)	1.2 (0.059 ... 8.7)	3.0 (-22 ... 28)
ERA5	227.475	3.0 (2.0 ... 8.0)	0.59 (0.17 ... 1.3)	-13 (-31 ... 7.1)
MSWEP	157.021	4.0 (2.0 ... 15)	0.45 (0.087 ... 1.6)	-20 (-42 ... 13)
CHIRPS	221.43	5.0 (5.0 ... 5.0)	**30 (2.2 ... 7.7e+4)**	**39 (0.35 ... 1.1e+2)**

4 Model evaluation

In this section we show the results of the model evaluation for the assessed region. The climate models are evaluated against the observations in their ability to capture:

1**. Seasonal cycles:** For this, we qualitatively compare the seasonal cycles based on model outputs against observations-based cycles (Figs A.2 & A.3). We discard the models that exhibit ill-defined peaks in their seasonal cycles. We also discard the model if the rainy season onset/termination varies significantly from the observations.

2. Spatial patterns: Models that do not match the observations in terms of the large-scale precipitation patterns (Figs A.4 & A.5) are excluded.

3. **Parameters of the fitted statistical models**. We discard the model if the model and observation parameters ranges do not overlap.

The models are labelled as 'good', 'reasonable', or 'bad' based on their performances in terms of the three criteria discussed above (Table 4.1). A model is given an overall rating of 'good' if it is rated 'good' for all three characteristics. If there is at least one 'reasonable', then its overall rating will be 'reasonable' and 'bad' if there is at least one 'bad'. The tables show the model evaluation results. Models that were rated 'good' and 'reasonable' were used: this resulted in 58 of 21 CMIP6 models, 3 of 6 CORDEX models, and 6 of 11 HighResMIP models being used in the analysis.

Table 4.1: *Evaluation results of the climate models considered for attribution analysis of Jun-Sep Rx30day. For each model, the threshold for a 1-in-5-year event is shown, along with the best estimates of the Dispersion and Shape parameters are shown, along with 95% confidence intervals. Furthermore evaluation of the seasonal cycle and spatial pattern are shown in the appendix.*

Model / Observations	**Seasonal cycle**	**Spatial pattern**	**Dispersion**	**Shape parameter**	**Conclusion**
Observations					
CPC			0.465 (0.357 ... 0.560)	-0.11 (-0.39 ... 0.049)	
IMERG			0.201 (0.108 ... 0.250)	0.086 (-0.50 ... 1.2)	
STATIONS			0.254 (0.194 ... 0.317)	-0.37 (-0.81 ... -0.12)	
MSWEP			0.239 (0.180 ... 0.285)	0.052 (-0.25 ... 0.27)	
CHIRPS			0.240 (0.145 ... 0.305)	-0.15 (-1.0 ... 0.092)	
Models					
CMIP6					
ACCESS-ESM1-5 ()	bad	good	0.218 (0.131 ... 0.292)	0.30 (-0.31 ... 1.0)	bad
CanESM5 ()	bad	bad	0.901 (0.667 ... 1.07)	0.34 (-0.15 ... 2.4)	bad

CESM2-WACCM ()	reasonable	good	0.468 (0.303 ... 0.558)	0.065 (-0.18 ... 0.53)	reasonable
EC-Earth3 ()	good	good	0.323 (0.213 ... 0.376)	-0.0078 (-0.58 ... 0.50)	good
EC-Earth3-CC ()	good	good	0.355 (0.248 ... 0.424)	-0.046 (-0.34 ... 0.29)	good
EC-Earth3-Veg-LR ()	good	good	0.399 (0.271 ... 0.476)	-0.041 (-0.63 ... 0.41)	good
FGOALS-g3 ()	bad	reasonable	0.370 (0.208 ... 0.456)	0.00029 (-0.31 ... 0.49)	bad
GFDL-CM4 ()	bad	good	0.301 (0.178 ... 0.385)	-0.16 (-0.63 ... 0.12)	bad
GFDL-ESM4 ()	bad	good	0.437 (0.296 ... 0.527)	0.032 (-0.69 ... 0.36)	bad
INM-CM4-8 ()	good	reasonable	0.318 (0.214 ... 0.382)	-0.37 (-0.76 ... 0.15)	reasonable
INM-CM5-0 ()	bad	reasonable	0.355 (0.249 ... 0.428)	-0.021 (-0.45 ... 0.28)	bad
IPSL-CM6A-LR ()	bad	good	0.311 (0.220 ... 0.367)	0.11 (-0.31 ... 0.52)	bad
KACE-1-0-G ()	bad	reasonable	0.479 (0.334 ... 0.569)	0.24 (-0.064 ... 0.62)	bad
KIOST-ESM ()	good	good	0.508 (0.334 ... 0.595)	0.10 (-0.54 ... 1.0)	good
MIROC6 ()	bad	reasonable	0.312 (0.179 ... 0.406)	0.47 (-0.11 ... 1.3)	bad
MPI-ESM1-2-HR ()	bad	reasonable	0.371 (0.181 ... 0.444)	0.18 (-0.22 ... 1.1)	bad
MPI-ESM1-2-LR ()	bad	reasonable	0.585 (0.408 ... 0.703)	-0.036 (-0.61 ... 0.19)	bad
MRI-ESM2-0 ()	bad	reasonable	0.499 (0.372 ... 0.591)	0.074 (-0.38 ... 0.39)	bad
NESM3 ()	bad	reasonable	0.680 (0.499 ... 0.842)	-0.16 (-0.45 ... 0.16)	bad
NorESM2-LM ()	good	good	0.442 (0.314 ... 0.533)	0.032 (-0.63 ... 0.52)	good
NorESM2-MM ()	reasonable	good	0.399 (0.273 ... 0.482)	0.33 (0.086 ... 0.75)	reasonable
CORDEX					
HadGEM2-ES_r1i1p1_GERICS-REMO2015 (1)	bad	reasonable	0.284 (0.209 ... 0.341)	-0.084 (-0.28 ... 0.13)	bad
MIROC5_r1i1p1_ORNL-RegCM4-7 (1)	bad	good	0.294 (0.234 ... 0.334)	0.039 (-0.16 ... 0.32)	bad
MPI-ESM-LR_r1i1p1_GERICS-REMO2015 (1)	good	reasonable	0.329 (0.272 ... 0.382)	0.065 (-0.25 ... 0.30)	reasonable
MPI-ESM-MR_r1i1p1_ORNL-RegCM4-7 (1)	good	good	0.243 (0.191 ... 0.281)	0.0047 (-0.21 ... 0.17)	good

NorESM1-M_r1i1p1_GERICS-REMO2015 (1)	good	reasonable	0.410 (0.317 ... 0.485)	0.072 (-0.45 ... 0.38)	reasonable
NorESM1-M_r1i1p1_ORNL-RegCM4-7 (1)	bad	good	0.302 (0.236 ... 0.354)	-0.094 (-0.34 ... 0.11)	bad
HIGHRESMIP (1)					
CMCC-CM2-HR4 (1)	bad	reasonable	0.247 (0.202 ... 0.274)	-0.018 (-0.21 ... 0.18)	bad
CMCC-CM2-VHR4 (1)	bad	reasonable	0.194 (0.164 ... 0.221)	-0.25 (-0.44 ... -0.063)	bad
CNRM-CM6-1 (1)	good	good	0.399 (0.322 ... 0.461)	-0.24 (-0.51 ... -0.14)	good
CNRM-CM6-1-HR (1)	good	good	0.304 (0.236 ... 0.363)	-0.26 (-0.53 ... -0.11)	good
EC-Earth3P (1)	good	good	0.231 (0.177 ... 0.273)	-0.28 (-0.51 ... -0.14)	good
EC-Earth3P-HR (1)	good	good	0.230 (0.182 ... 0.268)	-0.33 (-0.60 ... -0.18)	good
HadGEM3-GC31-HM (1)	good	reasonable	0.270 (0.206 ... 0.319)	-0.18 (-0.36 ... -0.072)	reasonable
HadGEM3-GC31-LM (1)	good	bad	0.328 (0.266 ... 0.373)	0.28 (0.097 ... 0.52)	bad
HadGEM3-GC31-MM (1)	good	bad	0.306 (0.251 ... 0.343)	0.024 (-0.23 ... 0.22)	bad
MPI-ESM1-2-HR (1)	good	good	0.272 (0.210 ... 0.322)	-0.24 (-0.49 ... -0.098)	good
MPI-ESM1-2-XR ()	good	good	0.213 (0.170 ... 0.245)	-0.20 (-0.35 ... -0.038)	good

5 Multi-method multi-model attribution

This section shows Probability Ratios and change in intensity ΔI between a past climate that is 1.3℃ cooler than now and the current climate for models that passed model evaluation and also includes the values calculated from the fits with observations. For all the models that passed the evaluation test, we show the results between the current climate and a future climate that is 1.3℃ warmer than now.

Table 5.1: *Event magnitude, probability ratio and change in intensity for a 5-year return period for Jun-Sep Rx30day for observational datasets and each model that passed the evaluation tests.* ***(a)*** *from pre-industrial climate to the present and* ***(b)*** *from the present to 2.6℃ above pre-industrial climate.*

		Current warming level [˚C]		**Future warming level [2.6˚C]**	
Model / Observations	**Threshold for return period 5 yr**	**Probability ratio PR [-]**	**Change in intensity ΔI [mm/30day]**	**Probability ratio PR [-]**	**Change in intensity ΔI [%]**
CPC	261.485 mm/30day	2.2e+2 (2.6 ... 1.4e+8)	93 (14 ... 1.9e+2)		
IMERG	153.255 mm/30day	2.2 (0.71 ... 3.9e+2)	24 (-17 ... 98)		
STATIONS	319.886mm/30day	1.2 (0.059 ... 8.7)	3.0 (-22 ... 28)		
MSWEP	157.021 mm/30day	0.45 (0.087 ... 1.6)	-20 (-42 ... 13)		
CHIRPS	221.43 mm/30day	30 (2.2 ... 7.7e+4)	39 (0.35 ... 1.1e+2)		
CESM2-WACCM ()	2.3e+2 mm/30day	8.9 (3.2 ... 44)	79 (44 ... 1.3e+2)	1.5 (1.3 ... 1.8)	14 (10 ... 21)
EC-Earth3 ()	1.4e+2 mm/30day	0.92 (0.53 ... 1.7)	-1.8 (-15 ... 12)	1.1 (0.93 ... 1.3)	2.6 (-1.7 ... 6.3)
EC-Earth3-CC ()	1.5e+2 mm/30day	0.89 (0.58 ... 1.6)	-3.1 (-15 ... 12)	1.0 (0.83 ... 1.2)	0.28 (-4.9 ... 5.4)
EC-Earth3-Veg-LR ()	1.6e+2 mm/30day	1.7 (0.73 ... 6.3)	13 (-8.3 ... 37)	1.0 (0.82 ... 1.3)	0.80 (-4.3 ... 6.0)
INM-CM4-8 ()	1.2e+2 mm/30day	0.95 (0.50 ... 2.8)	-0.78 (-13 ... 14)	1.3 (0.98 ... 1.5)	4.0 (-0.27 ... 7.5)
KIOST-ESM ()	1.8e+2 mm/30day	2.4 (1.1 ... 6.2)	33 (4.3 ... 63)	1.5 (1.3 ... 1.8)	16 (9.6 ... 22)
NorESM2-LM ()	1.4e+2 mm/30day	10 (2.3 ... 1.0e+2)	92 (32 ... 1.7e+2)	1.9 (1.4 ... 2.4)	24 (14 ... 33)
NorESM2-MM ()	1.4e+2 mm/30day	2.4 (0.93 ... 7.8)	38 (-2.7 ... 1.0e+2)	1.5 (1.3 ... 1.9)	18 (9.0 ... 26)
MPI-ESM-LR_r1i1p1_GERICS-REMO2015 (1)	1.4e+2 mm/30day	0.71 (0.28 ... 11)	-9.1 (-34 ... 39)	1.0 (0.72 ... 1.4)	0.27 (-9.5 ... 9.8)
MPI-ESM-MR_r1i1p1_ORNL-RegCM4-7 (1)	2.9e+2 mm/30day	0.38 (0.23 ... 1.0)	-21 (-37 ... 0.70)	0.64 (0.38 ... 1.0)	-8.9 (-18 ... 0.13)
NorESM1-M_r1i1p1_GERICS-REMO2015 (1)	1.9e+2 mm/30day	1.6 (0.34 ... ∞)	14 (-35 ... 88)	1.1 (0.79 ... 1.6)	3.9 (-6.4 ... 14)
CMCC-CM2-VHR4 (1)	2.7e+2 mm/30day	1.9 (0.54 ... ∞)	12 (-14 ... 50)	(...)	(...)
CNRM-CM6-1 (1)	3.4e+2 mm/30day	3.4 (0.57 ... ∞)	16 (-10 ... 41)	(...)	(...)
CNRM-CM6-1-HR (1)	2.6e+2 mm/30day	2.2 (0.49 ... 23)	9.0 (-9.9 ... 26)	(...)	(...)

EC-Earth3P (1)	2.8e+2 mm/30day	1.1 (0.38 ... 9.7)	0.67 (-17 ... 16)	(...)	(...)
HadGEM3-GC31-MM (1)	1.9e+2 mm/30day	5.0 (0.62 ... ∞)	20 (-7.3 ... 48)	(...)	(...)
MPI-ESM1-2-HR (1)	2.0e+2 mm/30day	1.2 (0.42 ... 9.4)	2.1 (-14 ... 20)	(...)	(...)

6 Hazard synthesis

For the maximum 30-day rainfall within the monsoon season (JJAS), we evaluate the influence of anthropogenic climate change on the events by calculating the probability ratio as well as the change in intensity using observations and climate models. Models which do not pass the evaluation described above are excluded from the analysis. The aim is to synthesise results from models that pass the evaluation along with the observations-based products, to give an overarching attribution statement.

Figure 6.1 shows the changes in probability and intensity for the observations (blue) and models (red). Before combining them into a synthesised assessment, first, a representation error is added (in quadrature) to the observations, to account for the difference between observations-based datasets that cannot be explained by natural variability. This is shown in these figures as white boxes around the light blue bars. The dark blue bar shows the average over the observation-based products.

Next, a term to account for intermodel spread is added (in quadrature) to the natural variability of the models. This is shown in the figures as white boxes around the light red bars. The dark red bar shows the model average, consisting of a weighted mean using the (uncorrelated) uncertainties due to natural variability plus the term representing intermodel spread (i.e., the inverse square of the white bars).

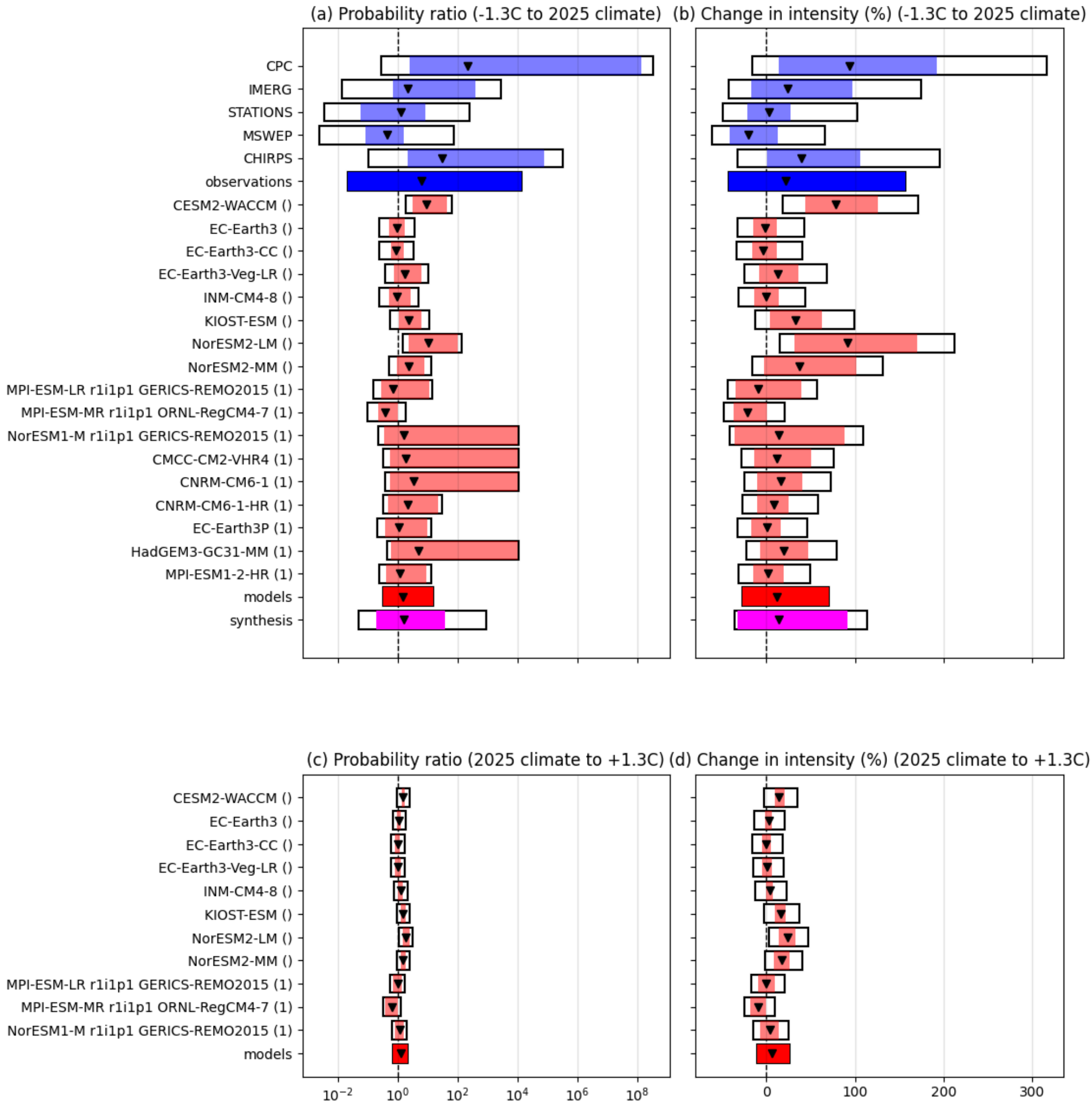

Figure 6.1*: Synthesis of* ***(a)*** *probability ratio and* ***(b)*** *intensity change when comparing JJAS Rx30day rainfall over the study region with a 1.3℃ cooler climate. Synthesis of* ***(c)*** *probability ratio and* ***(d)*** *intensity change when comparing JJAS Rx30day rainfall over the study region with a 1.3℃ warmer climate.*

Observation-based products and models are combined into a single result in two ways. Firstly, we neglect common model uncertainties beyond the inter-model spread that is depicted by the model average, and compute the weighted average of models (dark red bar) and observations (dark blue bar): this is indicated by the magenta bar. As, due to common model uncertainties, model uncertainty can be larger than the inter-model spread, secondly, we also show the more conservative estimate of an unweighted, direct average of observations (dark blue bar) and models (dark red bar) contributing 50% each, indicated by the white box around the magenta bar in the synthesis figures. The figures are also given in table 6.1.

Data	GMST		
	Time period	**Probability ratio (95% CI)**	**Intensity change (%) (95% CI)**
Observations	**Past- Present**	6.06 (0.0222 … 13800)	22.4 (-41.8 … 157)
Models		1.44 (0.318 … 15.7)	12.3 (-26.4 … 70.7)
Synthesis		1.61 (0.190 … 37.8)	14.7 (-31.8 … 92.2)
Models only	**Present- Future**	1.23 (0.719 … 2.09)	6.65 (-10.5 … 26.8)

Table 6.1: *Summary of results for JJAS Rx30day, presented in Figs 6.1-6.2: changes due to GMST include past-present changes and present-future changes. The numbers in red show estimates when the CESM2-WACCM and NorESM1-MM are not included in the attribution analysis*

The white boxes around the observations show that the different observational products are inconsistent with each other. The products that show more moderate increases, IMERG and CHIRPS, are closer to the station data, but neither of them is a good match to the station data in all locations where station data is available, thus we cannot confidently exclude MSWEP or CPC, both of which include satellite observations as well as numerical modelling. Thus, the uncertainty around the observations are high, but the best estimate, of a 22% increase, is in line with previous studies in the region, and given that a lot of the floods are the consequence of heavy daily rainfall, on wet soils, the Clausius-Clayperon relationship applies, providing the physical mechanism behind some of the observed increase in rainfall. Given that many individual stations and the observations best estimate are above the expected ~10% increase from Clausius-Clayperon alone, dynamical changes also likely play a role.

The models overall show smaller changes than most observations-based products, but with one exception show either an increase or effectively no-change, with a synthesised best estimate of 12%. In particular, two of the climate models included in this analysis, both known for their more realistic representation of aerosols and irrigation that are major factors influencing rainfall processes in this region, were found to show increases of 40-80%. Overall the synthesised result gives a best estimate of 15% increase in the intensity. Future simulations show a similar picture but overall smaller changes and high uncertainty, which is also in line with the published literature and IPCC projections.

The probability ratios show a higher discrepancy between observations and between observation-based products and models, as the numbers are more sensitive to the return time, yet they do overall show the same behaviour as the intensity changes.

Thus, we report the best estimate of the synthesised result of the intensity change as the main overarching result, highlighting that this might well be an underestimation and that the region needs to be prepared for even stronger increases in heavy rainfall, while also noting that higher variability and an increase in drier years, especially in the northern part of the region studied, cannot be excluded.

7 Vulnerability and exposure

Flooding in Pakistan is common during the monsoon season, with floods occurring nearly every year. Flooding in Pakistan results from riverine floods in the Indus basin, flash floods which typically occur in hilly areas of Baluchistan, Punjab, Kashmir and the Khyber-Paktunkhwa, and coastal floods often as result of cyclones (Tariq and de Giesen, 2011). Flash floods can be caused by intense local rainfall events and steep terrain, and are characterised by their rapid onset, high peak discharge and relatively localised spatial extent, which also makes them extremely impactful and difficult to predict in advance (AMS, 2017; WMO, 2006). During floods in 2010, 60% of the casualties in the Northwest Frontier were linked to flash floods (Tariq and de Giesen, 2011).

According to the National Disaster Management Authority, as of July 29, floods in Pakistan resulted in 288 deaths, including 136 children and 690 injuries, with Punjab and KP worst affected. Over 650 km of roads, 12 bridges, and 1,567 houses were damaged. Additionally, 327 livestock perished, highlighting the widespread humanitarian and infrastructural impact across the countries' main population centres (NDMA, 2025). This section explores the vulnerability and exposure factors that may have driven or mitigated risks associated with flooding.

7.1 Infrastructure, informality and land use

In Pakistan, in many areas, agricultural land has been converted into residential and commercial areas, reducing natural water absorption surfaces like wetlands and open spaces, and increasing surface runoff during heavy rains (National Institute for Disaster Management Pakistan, 2025). Between 2001 and 2022, land use changes along the Swati River—deforestation, bare land increase, and urban expansion—have intensified runoff, slope instability, and landslide risk on steep slopes, triggering landslides and higher debris flow that is particularly damaging (Bazei et al., 2025). Efforts to develop flood risk zones and hazard maps for 5- and 50-year floods have been made, but their implementation remains unclear (Tariq and de Giesen, 2011). Identified high-risk areas include Sindh, Punjab, and Gilgit-Baltistan and flash floods affect urban and rural settlements in the northeast due to poor drainage and unregulated construction driven by urbanization (Khan et al., 2021). Cities rely on outdated drainage systems often used for a mix of wastewaters, with limited capacity for stormwater absorption (National Institute for Disaster Management Pakistan, 2025, Ali et al., 2024, Malik et al., 2019). Resulting floods frequently disrupt infrastructure, including hospital services (National Institute for Disaster Management Pakistan, 2025), electricity, and WASH facilities, particularly in low lying areas and informal settlements, increasing the risk of infectious diseases (Malik et al., 2019, Unicef, 2025).

Pakistan is one of the fastest growing countries in South Asia in urbanization with the UN Population Division estimating more than 50% of the country's population to be living in urban centres by 2050 (UN, 2019). The rapid urbanisation is largely driven by rural-urban migration and has led to congestion, pollution, water shortages, and rising housing demand in cities (UN Habitat, 2023, National Institute for Disaster Management Pakistan, 2025). Pakistan has a housing backlog of 13 million units in 2025 (PMRC, 2023), and more cities are expanding in an unplanned and unmanaged way, where urban slums and conversion of green infrastructure into grey infrastructure is occurring at an exponential rate to house this migrating population (UNDP, 2019; ADB, 2024).

While Pakistan's Housing Policy is intended to prioritize middle and low income groups with the provision of affordable housing (MoHW, 2001; MoHW 2025), estimates show that 50% of the Pakistan's urban population resides in informal settlements known as "kacchi abadis"(UN-Habitat, 2023). For instance, Peshawar's built-up areas have doubled in 20 years (UN Habitat, 2023, Ali et al., 2024). These densely populated informal settlements occupy green spaces and riverbeds, lack building codes, drainage, and offer substandard living conditions, exacerbating the existing vulnerabilities of the people housed there (ADB, 2024, National Institute for Disaster Management Pakistan, 2025, Ali et al., 2024). Flash floods can rapidly sweep away buildings close to the river, with flood levels significantly higher in areas with buildings in floodplains (Bazei et al., 2025).

Homes built with locally available materials (e.g. mud) in informal settlements are particularly exposed as they can be swept away or collapse when exposed to fast-moving flood waters and strong winds (Dialogue Earth, 2022). Reports of damages to weak structured houses were reported from informal colonies such as the Rimsha Colony in Islamabad and Jharanwala area in Lahore (UCA News 2025, Tribune, 2025). This was further exacerbated by stagnant rainwater accumulating in narrow lanes and entering homes due to clogged drainage systems (UCA News, 2025). Between June 26th and July 29th 2025, approximately 1567 houses were damaged due to rainfall across Pakistan, of which 538 were completely destroyed (NDMA, 2025). The house damage not only left people without shelter but also claimed many lives. House collapse constituted the leading cause of fatalities during the event claiming the lives of 164 people (54.9% of the total death toll), including women and children, between the same one month time period (NDMA, 2025, Dawn, 2025). In contrast, drowning accounted for significantly fewer casualties, with 50 reported deaths.

However, not all self-built homes are vulnerable to floods, bamboo houses with cross-bracing and lime plinths raised above ground have shown better flood resilience and are increasingly used in Sindh and Balochistan after recent floods (Dialogue Earth, 2022; UNESCO, 2024). Furthermore, research shows many households in floodplains have lived there for generations, view them as ancestral land, and often know evacuation routes and safe zones (Khawaja et al., 2024, Rana and Routrai, 2018). While residents display resilience and have endured past floods with minimal harm, risk perception remains low in some areas, especially among new migrants with less experience in self-evacuation (Khawaja et al., 2024). Additional vulnerabilities stem from the high presence of chronically at-risk populations in informal settlements. In Rawalpindi, Sialkot, and Muzaffargarh (Punjab), one in five households (22%) includes members with chronic illness, disabilities, or pregnancy (Rana and Routrai, 2018).

In some areas, informal settlements around water ways were at risk of inundation. The France Colony located around the banks of Nullah Lai, reported dangerously high levels of water in the nullah after heavy downpour on July 17th 2025 (UCA News, 2025). As the water levels in the Nullah rose to 15 feet, close to the 20 feet critical mark, residents were advised to evacuate to avoid danger in case the Nullah overflowed (Daily Times, 2025; Radio Pakistan, 2025). However, many of them reported restraints as they had nowhere else to go (UCA News, 2025). Not only is the proximity to Nullah Lai worsening the vulnerability of the residents, but the construction is also narrowing the width of natural water passageway the nullah is supposed to offer, thereby increasing the risk of exposure of low lying areas to flash floods in case of heavy rain (Dawn, 2025). Similar issues are being faced along other waterways including the Saidpur Nullah and the Korang Nullah in Islamabad, putting surrounding populations at risk (Dawn, 2025).

Research suggests that within Pakistan, approximately 22 million slum dwellers reside in flood plains (Li et al, 2022). Across the globe South, within such formally unrecognized settlements, limited access to social services and poor quality of infrastructure severely impacts response to flooding (Carbon Brief, 2025). Combined with physical exposure, these vulnerabilities heighten the flood risk faced by informal slum communities. The rising number of casualties and damages associated with the floods of 2025 highlights the urgent need for improved urban planning, and better management of informal settlements and buildings near riverbeds, particularly in the KP and Punjab (NDMA, 2024)

7.2 Agriculture

Agriculture is a major part of Pakistan's economy, accounting for approximately 24% of GDP in 2025 (Pakistan Bureau of Statistics, 2025). The state of Punjab, which has seen amongst the highest impacts from the floods, produces more than half of the country's agricultural output and 25% of its labor force is engaged in agricultural activities (Sardar, A. et al, 2025). The floods are having an impact on cotton, rice, maize, and mango crops, some of which are key export crops or provide the raw materials for other exports (e.g. cotton for textiles) and are likely to have an impact on GDP (Arab News, 2025). One study modeled the economic impacts of a 5-year flood, similar to the event described in this study and found that it could cost the country's GDP about $20.4 billion, with 8.4 million people at risk (Khan et al., 2021).

Past flood disasters have had a significant impact on agriculture. For example the 2014 flash floods resulted in over 1 million acres of cropland and 250,000 farmers affected as they lost crops and fodder. In Pakistan 'Bait' areas are places where temporary islands form within the area of a river. Bait communities, who depend on agriculture and livestock for their livelihoods, and often live along flood-prone riverbanks, are more vulnerable (Ahmed and Afzal, 2022). Floods affect their food security, health, access to water, and ability to conduct their livelihoods (Ahmed and Afzal, 2022).

7.3 Flood risk management

In 1977, a Federal Flood Commission was established, and in 1978, a national flood risk management plan (NFPP) was developed as a response to the deadly 1973 floods that led to ~2billion USD in damage and 474 deaths (Tariq and de Giesen, 2011). Flood risk management includes a combination of flood protection structures (e.g. embankments, studs and spurs alongside rivers), and flood forecasting. In Punjab and Khyber Pakhtunkhwa (KP), small dams and embankments have been built under provincial flood protection programmes, and along parts of the Indus Basin, river channelization has been applied to manage flood control (Khan et al., 2021).

The Pakistan Meteorological Department (PMD) has a flood forecasting system and issues early warnings (Tariq and de Giesen, 2011). For this event, the Pakistan Meteorological Department (PMD) and the National Disaster Management Authority (NDMA) had issued warnings ahead of the rainfall spell that began around 16 July, following the development of a low-pressure area (LPA) over northwest Madhya Pradesh, India. This system was forecast to move into Pakistan within the next 48 hours, bringing strong monsoon currents into the central and northern regions of the country. This system, combined with an existing westerly wave, was forecast to produce heavy rain, strong winds, and thunderstorms across Khyber Pakhtunkhwa, Punjab, Kashmir, Gilgit-Baltistan, Islamabad, and northeastern and southern Balochistan. The PMD projected scattered heavy to very heavy rainfall in several regions, including Islamabad, KP, Punjab, and northeastern Balochistan, prompting concerns about potential landslides and mudslides in hilly areas such as Murree, Galliyat, Kashmir, and Gilgit-Baltistan. Urban flooding was also anticipated in low-lying parts of cities like Rawalpindi, Lahore, Gujranwala, and Peshawar. Radar systems have been installed in and around the Jhelum river and other flash flood prone areas to detect heavy rainfall events like those observed this year (Tariq and de Giesen, 2011). On 16 July, the Flood Forecasting Division (FFD) predicted an exceptionally high flood in the Jhelum River at Mangla, with water flow expected to range between 350,000 and 450,000 cusecs. The tributaries of the Jhelum River were also expected to reach dangerously high levels (ReliefWeb, 17 July 2025). Residents living along the low-lying flood plains of the Lai Nullah channel that runs through Rawalpindi were asked to evacuate on account of rising water levels (Phys.org, 17 July 2025). Warnings and evacuation orders for high risk areas were communicated from mosques (Arabnews, 2025). In response, the NDMA called on provincial and district administrations to activate emergency response teams, ensure the availability of rescue equipment, and clear drainage systems in urban areas. Tourists had been advised to avoid high-altitude regions during the period of expected heavy rainfall (Arab News, 14 July 2025). Literacy among residents in flood plains (Lahore) remains low, and especially for those who have migrated, making risk communication difficult (Khawaja et al., 2024). In urban communities in Pakistan past experiences and hazard proximity significantly influence risk perception to flood hazards (Rana et al., 2020).

The recent rainfall events and the reporting surrounding it has also highlighted new actors that have entered the weather and climate space, complicating important messaging around extreme weather. In July, a private organization, 'Weather Walay', claimed that a cloudburst resulted in 423mm of rainfall in Chakwal, based on their automated weather stations. This claim was picked up by the national news outlets without verification, reflected in social media posts, and was later re-reported by the international media (Khan & Saeed, 2025). Later Pakistan's Meteorological Department, which is mandated to provide meteorological expertise and services, rejected the claims of a cloudburst and reported that their stations showed 142.2 mm rainfall in Chakwal (APP, 2025). The inaccurate reporting and narrative building around a disaster could lead to public confusion and misdirect emergency response services. Moreover, the resulting ambiguous information generated around hazards can erode the public's trust in forecasts, early warning systems, and reporting putting vulnerable populations at a higher risk. This is not only an issue in Pakistan as private weather companies are proliferating around the world. The World Meteorological Organisation has encouraged collaboration through public-private partnerships that help bolster trust in forecasts rather than erode it (WMO, 2019).

7.4 Tourism

Many media reports highlight tourist casualties linked to monsoon rainfall in Northern Pakistan, which is a recreational hotspot especially in the summer months (Ullah et al., 2024). Tourists are often unfamiliar with the harsh weather events that could occur during their visits including flashfloods, GLOFs, landslides and associated road blockages.

Towards the end of June, the flash floods in Swat River wreaked havoc when the river swept away a 16 member family having breakfast at the river side (Al-Jazeera, 2025; The Guardian, 2025).

Moreover, at least 10 people died near the Swat Bypass Hotel (Dawn, 2025a). The flood also damaged parts of the Karakoram Highway (KKH) further stranding several tourists (Dawn, 2025c). Rescue operations were required following flooding in Naran, Jalkhad, Barwai and Besar (Dawn, 2025e).

The NDMA periodically published weather advisories detailing the hazard and the region of concern, and warnings communicating that the tourists should remain cautious, check weather updates before travelling, avoid trekking on ice, or getting close to glaciers amidst GLOF warnings, tourists surged to the Northern areas (NDMA, 2025). Road closures owing to disasters along with patchy communication services in these regions (Arab News, 2024), which are disrupted during monsoon season (Dawn, 2025c) can derail rescue services. Disruptions in early warning systems can also hinder communication (Dawn, 2025g).

Tourism, despite being a significant contributor to Northern Pakistan's economy, can exacerbate the exposure and vulnerabilities to climatic impacts (Ali, 2023). Infrastructure such as hotels, rest houses, restaurants, bridges are often constructed close to river beds in flood-risk zones. This unregulated construction puts the lives of tourists at risk (Culture Unplugged, 2025; Dawn, 2025h). The proximity to the river leaves a small response window in case a disaster strikes thereby exacerbating risk. Proactive action to ensure locals' and tourist safety is required, as without it evacuation and rescue services become increasingly stretched.

7.5 Adaptation, Losses and Damages

Following the 2022 floods that swept across Pakistan, the narratives from the country proved instrumental in advocating for the landmark decision on formation of Loss and Damage Fund that came during COP27. The devastating floods of 2022, shook the economy of the country bringing damages to US$14.9 billion and losses to US$15.2 billion (GoP, 2022). To cover the most urgent needs, the Flood Response Plan estimated the requirements of US$816 million to enable urgent multi-sectoral humanitarian response to 9.5 million people until 31 May 2023 (UNDP, 2022). As of yet, 76.1% of the required finance has been delivered (OCHA, 2025). Apart from the urgent requirements, the recovery and reconstruction needs were estimated to amount to US$16.3 billion(GoP, 2022).

For reconstruction and rehabilitation, donors also provided financial assistance to Pakistan. For example, the Sindh Peoples Housing for Flood Affectees Project, aims at restoration and reconstruction of multi-hazard resilient housing units to the 2022 flood affectees in 24 districts of Sindh by the year 2027 (ADB, 2024). Donors have committed financial support through loans for this project, including $950 million from the World Bank, $400 million from the Asian Development Bank, and $200 million from the Islamic Development Bank (World Bank, 2024) (ADB, 2024) (IsDB, 2025). These contributions fall short of the full value, amounting 2.036 billion, required for this reconstructive work addressing the basic needs of housing for flood victims (GoS, 2025). Simultaneously, the required size of the finance needed for resilient recovery, reconstruction, and rehabilitation, is beyond the fiscal capacity of Pakistan's government and would require significant international support (GoP, 2022). The situation mirrors the overall climate finance needs gap in Pakistan, especially with respect to adaptation financing. The World Bank estimates that the country would need US$ 348 billion between 2023 and 2030 to address its adaptation and mitigation needs, while the available domestic finance and the international assistance remain limited in comparison

(World Bank, 2022). Moreover, international finance, which is critical in addressing adaptation needs, not only remains insufficient but also tends to favour mitigation focused interventions (FCDO, 2024).

Recent events once again serve as a stark reminder that climate change produces impacts that are beyond Pakistan's ability to cope, especially when development is uninformed and adaptation efforts remain underfunded. The factors that contributed to losses and damages during the 2022 floods largely persisted in 2025. In 2022, floodwaters in Swat River inundated riverbeds, leading to significant loss of infrastructure constructed along the river banks (Tribune, 2022). A similar pattern was observed in 2025, as floodflows once again swept away people and inundated hotel buildings (Reuters, 2022; Daily Times, 2025). Furthermore, construction along water ways continues to obstruct the natural path of waterflow resulting in urban flash floods during extreme rainfall events. This issue was observed in 2021 in Islamabad and again in 2025 (Dawn, 2022; TRT, 2025). Similar issues of drainage blocks were observed in other parts of Pakistan such as the Larkana floodplain in Sindh during the 2022 floods (Cui, P et al., 2025). These avoidable impacts underscore the urgent need for adaptive measures that, once in place, could significantly reduce losses and strengthen Pakistan's climate resilience amidst recurring climatic events, especially floods. However, the effectiveness of adaptation is contingent on the scaling up of financial assistance, for which international support is imperative, and on integrating scientific evidence into resilience planning which is essential for anticipating, managing, and reducing climate risks with greater precision and impact.

Data availability

All time series used in the attribution analysis will be made available through the Climate Explorer.

References

All references are given as hyperlinks in the text.

Appendix

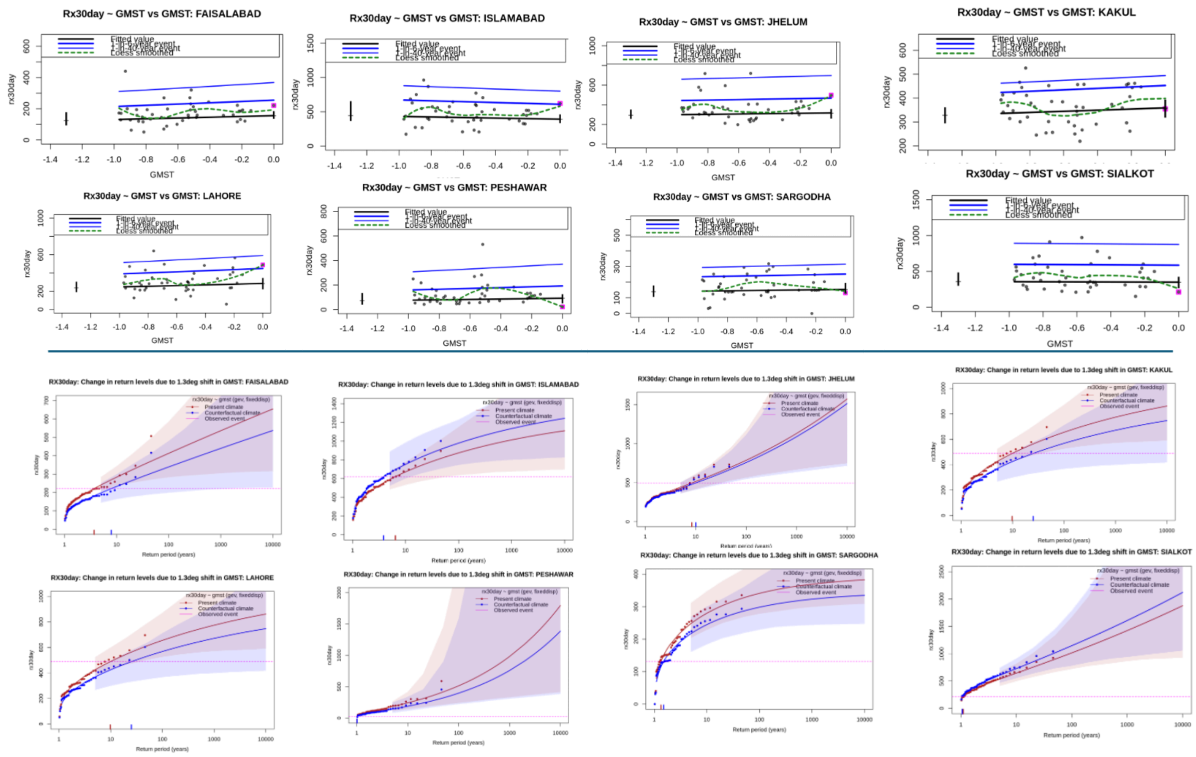

Figure A.1: *GEV fit with fixed dispersion parameter scaling proportional to GMST of the index series.* ***(a-f)*** *Observed JJAS Rx30day [mm/30day] as a function of the smoothed GMST. The thick black line denotes the time-varying location parameter. The vertical black lines show the 95% confidence interval for the location parameter, for the current, 2025 climate and the fictional, 1.3ºC cooler climate. The 2025 observation is highlighted with the magenta box.* ***(g-l)*** *Return time plots for the climate of 2025 (red) and a climate with GMST 1.3 ºC cooler (blue). The past observations are shown twice: once shifted up to the current climate and once shifted down to the climate of the pre-industrial era. The markers show the data and the lines show the fits and uncertainty from the bootstrap. The magenta line shows the magnitude of the 2025 event analysed here. These are shown for the 8 stations provided by PMD: Faisalabad, Islamabad, Jhelum, Kakul, Lahore, Peshawar, Sargodha and Sialkot.*